Effects of GH_2/LOX Velocity and Momentum Ratios on Shear Coaxial Injector Atomization

M. Ferraro,* R. J. Kujala,* J.-L. Thomas,†
M. J. Glogowski,‡ and M. M. Micci§
The Pennsylvania State University,
University Park, Pennsylvania 16802

Introduction

SHEAR coaxial injectors are currently found in liquid propellant rocket engines that use liquid oxygen and hydrogen as the propellants, such as the Space Shuttle Main engine (SSME) and the first stage Ariane 5 Vulcain engine. Liquid oxygen is injected into the combustion chamber through a central tube while hydrogen in a gaseous form is fed through an outside annular passage at a high velocity relative to the liquid jet. Impelled by liquid turbulence and gas-to-liquid interfacial interactions, liquid is stripped from the jet and entrained into the surrounding shear flow where the liquid ligaments and droplets experience further breakup and atomization. The resulting spray then vaporizes and mixes with the gaseous fuel to produce a volatile mixture for combustion.

There have been several previous experimental investigations to measure droplet sizes and velocities produced by shear coaxial injectors by means of phase Doppler interferometry where the fuel and oxidizer simulants were evaporating or combusting. Sankar et al.[1] analyzed a GN_2/LN_2 spray for both a shear coaxial and quadruplet injector. The gas pressure and liquid injection post recess were varied for the shear coaxial injector. Data were presented for the mean axial velocity and Sauter mean diameter for different locations in the spray. They found no definite relationship between the recess and atomization. However larger gas pressures, or higher gas velocities, improved atomization.

Glogowski et al.[2] examined shear coaxial sprays with both an air/water system and a GN_2/LN_2 system. The injector design was based on the SSME injector. They measured droplet velocity and diameter with the phase Doppler particle analyzer (PDPA) for both air/water and GN_2/LN_2. The GN_2/LN_2 tests looked at the effect of mixture ratio and chamber pressure past the critical pressure of nitrogen and showed improved atomization with lower mixture ratios.

Pal et al.[3] also modeled their injector after the SSME rocket injector. The paper included a comparison of PDPA data from air/water and liquid-oxygen/gaseous-hydrogen experiments. Both tests were run with similar flow conditions except for the Reynolds and Weber numbers and the ambient pressure. The authors found that Sauter mean diameters from the hot-fire experiments were larger than those from the cold-flow experiments. The mean droplet velocity was smaller for the GH_2/LOX tests than for the air/water tests. The purpose of this study was to measure LOX droplet sizes as a function of the relative velocity between the LOX and the hydrogen under combusting conditions.

Received 2 January 2001; revision received 5 July 2001; accepted for publication 4 August 2001.

*Graduate Research Assistant, Department of Aerospace Engineering and Propulsion Engineering Research Center. Student Member AIAA.

†Adjunct Research Associate, Department of Aerospace Engineering and Propulsion Engineering Research Center; currently Staff Engineer, SEP, Vernon, France. Member AIAA.

‡Graduate Research Assistant, Department of Aerospace Engineering and Propulsion Engineering Research Center; currently Staff Engineer, Lockheed Martin Space Systems Company, Sunnyvale, CA. Member AIAA.

§Professor, Department of Aerospace Engineering and Propulsion Engineering Research Center. Associate Fellow AIAA.

Experiment

Shear Coaxial Injector Element

The baseline dimensions of the injector used in this study are derived from the dimensions of the prototype injector element of the fuel preburner to the SSME although the operating conditions are different. The fuel annulus diameter is 5.03 mm, and the LOX post outer and inner diameters are 3.76 and 2.26 mm, respectively. The LOX post is recessed 2.54 mm into the injector element. To determine the injection properties of the gas, the temperature along with the fluctuating and mean components of the pressure are measured in the fuel plenum region. Likewise the pressure and temperature of the liquid are measured in the supply line at the entrance to the LOX post. The injector segment is separated into two concentric brass sections. The forward section contains a threaded insert that forms the outer diameter of the fuel annulus and can be replaced between tests without complete chamber disassembly in order to change the fuel velocity without changing its mass flow rate. The rear section provides the coupling of the injector to the propellant feed system.

Hot-Fire Experiment

The subscale combustion chamber was modular in design, allowing for simple variation of the chamber length, location of optical access, injector design, and throat diameter. The individual chamber segments include the injector, window, igniter, blank, and nozzle segments. With all segments in place, the interior length of the combustion chamber measures 25.7 cm. The chamber is designed to operate for 4 s at steady-state chamber pressures up to 10 MPa. The window segment is intended for droplet size and velocity measurements within the liquid oxygen spray using an Aerometrics PDPA. To reduce or eliminate contaminants from collecting on the windows during engine testing, a purge gas section was incorporated into the design of the window segment. Eight small holes inject nitrogen gas across the inner surface of the windows within the window recess region. Preliminary tests with the window segment located at the chamber midsection verified adequate window purging with nitrogen flow rates less than 10% of the total propellant flow rate. Measurements of the chamber inner surface temperature and the steady and oscillating components of chamber pressure are made in this segment.

The nozzle segment houses a water-cooled nozzle throat insert that is sized for a specific mass flow rate and chamber pressure. A stainless-steel flange retains the insert within the nozzle segment while serving a second function as a pressure relief mechanism. Propellant ignition is accomplished with a gaseous-oxygen/gaseous-hydrogen torch igniter. Both gases are introduced into a small combustion chamber attached to the side of the igniter segment and ignited by a high-voltage, electrical discharge. The resulting flame is drawn into the main chamber to ignite the main propellant and is then turned off when main chamber ignition is achieved.

Results and Discussion

For the hot-fire experiments that were conducted, mixture ratios ranged from 3.4 to 5.0, which resulted in velocity ratios between 11.1 and 30.1. However the majority of the tests were conducted with a mixture ratio of approximately 4.25. Different mixture ratios were achieved by varying the gaseous-hydrogen flow rate and holding the LOX flow rate constant at 0.113 kg/s, the actual SSME LOX flow rate. Chamber pressures ranged from 2.0 to 4.3 MPa. All tests were conducted at chamber pressures below the critical pressure of pure oxygen (~5 MPa).

Figure 1 shows the LOX droplet arithmetic mean diameter D_{10} vs the velocity ratio. The accuracy of the droplet diameter measurements was 3.3 μm. All measurements were taken along the axis at a distance of approximately 12 cm downstream of the injector face. Closer to the injector the spray was too dense to obtain PDPA measurements. A dramatic increase in the arithmetic mean diameter can be seen as the velocity ratio drops below a value of 12. The LOX droplet area mean diameter D_{20} displays the identical behavior. Figure 2 shows the LOX droplet velocity measured with an accuracy of 1.5 m/s as a function of the velocity ratio for the same

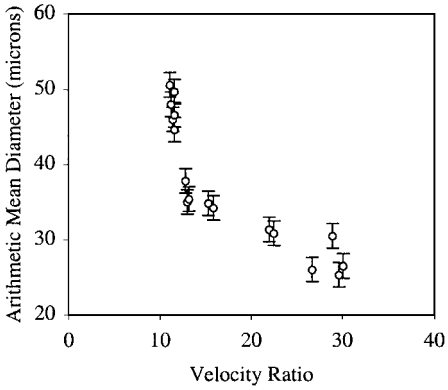

Fig. 1 LOX droplet arithmetic mean diameter as a function of gas/liquid velocity ratio (chamber pressures from 2.0 to 4.5 MPa).

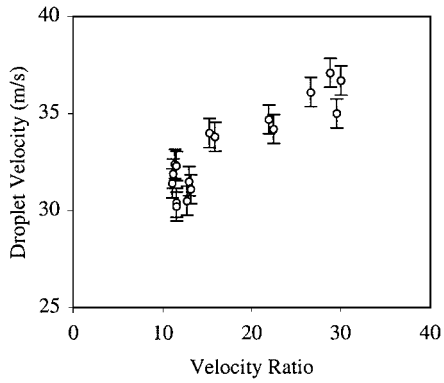

Fig. 2 LOX droplet axial velocity as a function of gas/liquid velocity ratio (chamber pressures from 2.0 to 4.5 MPa).

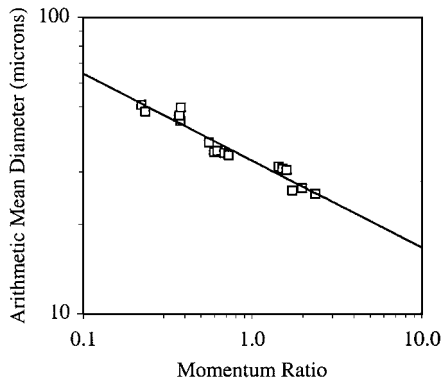

Fig. 3 LOX droplet arithmetic mean diameter as a function of gas/liquid momentum ratio (velocity ratios from 11.1 to 30.1).

tests. It can be seen that the droplet velocity increases linearly with the velocity ratio. The droplet velocity for low velocity ratios is approximately equal to the LOX injection velocity of 30 m/s. Radial scans made at several pressures showed the largest droplets along the axis of the spray with the drop size decreasing as one moved away from the axis. The droplet velocity was found to increase linearly with radial distance, moving from the slow moving liquid core to the high velocity gas stream.

Analysis of the experimental data showed that the arithmetic mean diameter measured along the axis at a distance of approximately 12 cm downstream of the injector face correlates well with the gas/liquid momentum ratio, defined here as

$$M_r = \rho_g U_g^2 \Big/ \rho_l U_l^2 \tag{1}$$

Figure 3 depicts the arithmetic mean diameter as a function of momentum ratio on a log-log scale, showing that the data lie closely

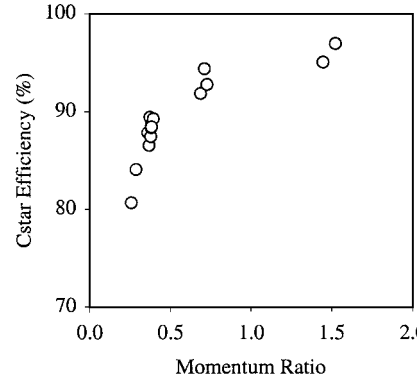

Fig. 4 c^* efficiency as a function of gas/liquid momentum ratio (velocity ratios from 11.1 to 30.1).

along a line for momentum ratios between 0.2 and 2.4. A curve fit applied to these data results in the expression

$$D_{10} = 33.2 M_r^{-0.296} \tag{2}$$

for the dependence of arithmetic mean diameter on momentum ratio M_r at the measurement location for the pressures just given. In particular, the droplet sizes that this expression predicts for pressures greater than 4.5 MPa do not match experimental results, indicating that pressure has a much greater effect on atomization as the critical point is approached.

Figure 4 shows the c^* efficiency plotted vs the momentum ratio for the tests performed between 2.5 and 3.0 MPa using a 1.16-cm-diam nozzle throat. The actual c^* was calculated from the measured chamber pressure and the fuel, oxidizer and purge gas flow rates while the theoretical c^* was calculated using the NASA Glenn CET93 equilibrium code.[4] As can be seen in Fig. 4, the result of a lower momentum ratio is a reduction in the combustion efficiency for the subscale rocket combustion chamber, probably as a result of the larger LOX drop sizes. Using the actual values of the c^*, calculated chamber residence times ranged from 1.5 to 2.0 ms. Lafon et al.[5] computed the lifetime of a 50-μm LOX droplet at the same chamber conditions as those obtained in these experiments to be approximately 4 ms. The measured droplet diameters varied by a factor of two, thus droplet lifetimes varied by a factor of four. Thus the predicted droplet lifetimes are of the same order as the calculated chamber residence times, and a factor of four change in the droplet lifetime could easily result in incomplete combustion for the larger droplet sizes.

Conclusions

A subscale rocket combustion chamber was operated with a single full-size SSME preburner element at a liquid oxygen flow rate of 0.113 kg/s. The effect of gas/liquid velocity and momentum ratios on LOX droplet size and velocity distribution was examined with a PDPA for mixture ratios between 3.2 and 5.6. Droplet sizes were found to decrease with increasing gas/liquid velocity or momentum ratio while the droplet velocities increased. The c^* efficiency was found to increase with increasing velocity and momentum ratios. A correlation was presented to predict the droplet arithmetic mean diameter as a function of gas/liquid momentum ratio for chamber pressures between 2.0 and 4.5 MPa.

Acknowledgments

This work was supported by U.S. Air Force Office of Scientific Research Grant F49620-95-1-0184, NASA Grants NAGW-1356, Supplement 10 and NGT-10034, and the Societe Europeene de Propulsion.

References

[1] Sankar, S. V., Brena de la Rosa, A., Isakovic, A., and Bachalo, W. D., "Experimental Investigation of Rocket Injector Atomization," *28th JANNAF Combustion Subcommittee Meeting*, Vol. II, Chemical Propulsion Information Agency Pub. 573, Columbia, MD, 1991, pp. 187–198.

[2]Glogowski, M., Bar-Gill, M., Puissant, C., Kaltz, T., Milicic, M., and Micci, M., "Shear Coaxial Injector Instability Mechanisms," AIAA Paper 94-2774, June 1994.

[3]Pal, S., Moser, M. D., Ryan, H. M., Foust, M. J., and Santoro, R. J., "Shear Coaxial Injector Atomization Phenomena for Combusting and Non-Combusting Conditions," *Atomization and Sprays*, Vol. 6, No. 2, 1996, pp. 227–244.

[4]McBride, B. J., Reno, M. A., and Gordon, S., "CET93 and CETPC. An Interim Updated Version of the NASA Lewis Computer Program for Calculating Complex Chemical Equilibria with Applications," NASA TM-4557, March 1994.

[5]Lafon, P., Yang, V., and Habiballah, M., "Supercritical Vaporization of Liquid Oxygen Droplets in Hydrogen and Water Environments," *Journal of Fluid Mechanics* (submitted for publication).

Equation for Additive Drag Coefficient at Static Conditions

K. L. Christensen*
KC Consulting Engineering, Rolla, Missouri 65401

Introduction

CALCULATION of additive drag at static conditions is usually not a problem simply because multiplying the drag coefficient by the dynamic pressure (which is zero at static conditions) is always zero. However, in some computer codes, if the additive drag coefficient is determined by dividing the additive drag force by the dynamic pressure, a zero divide error can result at static conditions. This problem is eliminated if the drag coefficient at static conditions is determined independently of the dynamic pressure. This technical Note describes how such an expression was derived from an existing additive drag coefficient equation.

Procedure

To use freestream velocity in the determination of airbreathing propulsion thrust, the system boundary is extended forward of the inlet cowl so that freestream velocity air crosses the system boundary. This requires that the drag component attributable to the airstream ahead of the inlet is included in determining the overall engine thrust. The nomenclature as used in this Note and in Ref. 1 is shown in Fig. 1.

The additive drag coefficient is calculated in Ref. 1 from

$$Cd_{\text{pre}} = \left[(P_c - P_\infty)A_c + \rho_c V_c^2 A_c - \rho_\infty V_\infty^2 A_\infty\right] \Big/ q_\infty A_c \qquad (1)$$

where P_c is static pressure at the cowl lip, P_∞ is freestream static pressure, A_c is the cowl lip area, ρ_c is the air density at the cowl lip, V_c is the air velocity at the cowl lip, ρ_∞ is the freestream air density, V_∞ is the freestream air velocity, A_∞ is the capture area of freestream flow, and q_∞ is the freestream dynamic pressure. However, because $q_\infty = 0$ when $M_\infty = 0$, this expression becomes indeterminate at static conditions. Yet the plot of Cd_{pre} as a function of A_∞/A_c and M_∞ (see page 196 in Ref. 1) shows finite values of Cd_{pre} values for $M_\infty = 0$. Therefore, all of the variables on the right side of Eq. (1) should be definable in terms of A_∞/A_c and M_∞. However, as will be shown, the desired expression of Cd_{pre} as a function of A_∞/A_c and M_∞ only is not possible. Ultimately, application of L'Hopital's rule will be required to obtain the desired expression for Cd_{pre} at static conditions.

Received 13 December 2000; accepted for publication 7 July 2001.

*President.

The first step is to rewrite Eq. (1) as the sum of three terms

$$Cd_{\text{pre}} = \frac{(P_c - P_\infty)A_c}{q_\infty A_c} + \frac{\rho_c V_c^2 A_c}{q_\infty A_c} - \frac{\rho_\infty V_\infty^2 A_\infty}{q_\infty A_c} \qquad (2)$$

which is simplified to

$$Cd_{\text{pre}} = \frac{P_c}{q_\infty} - \frac{P_\infty}{q_\infty} + \frac{\rho_c V_c^2}{q_\infty} - \frac{\rho_\infty V_\infty^2 A_\infty}{q_\infty A_c} \qquad (3)$$

Note that A_∞/A_c now appears explicitly in the third term. Also

$$q_\infty = \tfrac{1}{2}\rho_\infty V_\infty^2, \qquad \rho_c V_c^2 = \gamma M_c^2 P_c \qquad (4)$$

Therefore, substituting Eq. (4) into Eq. (3) gives

$$Cd_{\text{pre}} = \frac{P_c}{\frac{1}{2}P_\infty \gamma M_\infty^2} - \frac{P_\infty}{\frac{1}{2}P_\infty \gamma M_\infty^2} + \frac{\gamma P_c M_c^2}{\frac{1}{2}P_\infty \gamma M_\infty^2} - \frac{\rho_\infty V_\infty^2 A_\infty}{\frac{1}{2}P_\infty \gamma M_\infty^2 A_c} \qquad (5)$$

which becomes

$$Cd_{\text{pre}} = \frac{2P_c}{P_\infty \gamma M_\infty^2} - \frac{2}{\gamma M_\infty^2} + \frac{2P_c M_c^{\,2}}{P_\infty M_\infty^2} - 2\left(\frac{A_\infty}{A_c}\right) \qquad (6)$$

or

$$Cd_{\text{pre}} = \frac{2}{\gamma M_\infty^2}\left(\frac{P_c}{P_\infty} - 1\right) + \frac{2P_c M_c^2}{P_\infty M_\infty^2} - 2\left(\frac{A_\infty}{A_c}\right) \qquad (7)$$

Next, note that

$$P_c/P_\infty = (P_c/P_T)/(P_\infty/P_T) \qquad (8)$$

where P_T is the stagnation pressure for isentropic flow from freestream conditions to the cowl entrance. Then, because the ratio of static to total pressure for isentropic flow can be written as

$$P/P_T = \{1 + [(\gamma - 1)/2]M^2\}^{\gamma/(1-\gamma)} \qquad (9)$$

therefore,

$$\frac{P_c}{P_\infty} = \frac{\left\{1 + [(\gamma - 1)/2]M_c^2\right\}^{\gamma/(1-\gamma)}}{\left\{1 + [(\gamma - 1)/2]M_\infty^2\right\}^{\gamma/(1-\gamma)}} = \left\{\frac{1 + [(\gamma - 1)/2]M_c^2}{1 + [(\gamma - 1)/2]M_\infty^2}\right\}^{\gamma/(1-\gamma)} \qquad (10)$$

Also note that the freestream and cowl areas can be related by

$$A_c \big/ A^* = (A_c/A_\infty)\left(A_\infty \big/ A^*\right) \qquad (11)$$

where A^* is the cross-sectional flow area where $M = 1$ for isentropic flow. Then with

$$\frac{A}{A^*} = \frac{1}{M}\left[\frac{2}{\gamma + 1}\left(1 + \frac{\gamma - 1}{2}M^2\right)\right]^{(\gamma+1)/2(\gamma-1)} \qquad (12)$$

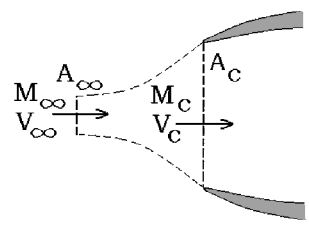

Fig. 1 Inlet nomenclature.